

The Role of Percent Volume Buried in the Characterization of Copper(I) Complexes for Lighting Purposes

Murat Alkan-Zambada ^{1,*}, Edwin C. Constable ² and Catherine E. Housecroft ²

¹ Laboratory of Inorganic Synthesis and Catalysis, Institute of Chemical Sciences and Engineering, École Polytechnique Fédérale de Lausanne (EPFL), ISIC-LSCI, BCH 3305, Lausanne 1015, Switzerland

² Department of Chemistry, University of Basel, BPR 1096, Mattenstrasse 24a, CH-4058 Basel, Switzerland; Catherine.Housecroft@unibas.ch; edwin.constable@unibas.ch (E.C.C.); catherine.housecroft@unibas.ch (C.E.H.)

* Correspondence: murat.alkan@epfl.ch

Received: 20 May 2020; Accepted: 3 June 2020; Published: 6 June 2020

Academic Editor: Abel Santos

Abstract: The usefulness of percent volume buried ($\%V_{bur}$) as a readily quantifiable property is investigated with regard to $[Cu(NN)(PP)]^+$ complexes of interest for lighting purposes. Photoluminescence quantum yields (PLQYs) and single crystal X-ray structures of 100 reported compounds were assembled, $\%V_{bur}$ of the ligand systems were calculated and analyzed for correlations. We found that increased shielding of the central Cu(I) cation relying on shared contributions of both (NN) and (PP) ligand systems led to increased PLQYs. These findings are of relevance for future characterizations of Cu(I)-based complexes and their photophysical behavior in the solid-state.

Keywords: copper(I); photoluminescence quantum yield; crystal structure; percent volume buried ($\%V_{bur}$); empirical correlations

1. Introduction

Ionic transition metal complexes (iTMCs) are widely present in chemistry for e.g., catalysis or lighting purposes. Understanding of the electronic and steric effects of ligands on the iTMCs is essential to improve rational design of iTMCs for their varied purposes. While quantifying electronic effects of ligands onto metal complexes can be performed by spectroscopic methods such as IR, [1] similar quantification of the steric impact is less straight-forward. Tolman cone-angles have been introduced for the calculation of steric parameters [2] and widely used but suffer limitations as its usefulness is greatly diminished when applied to more elaborate mono- or bi-dentate ligands. Consequently, Nolan and Cavallo introduced the percent volume buried ($\%V_{bur}$) as a quantifiable parameter to describe any given ligand [3]. The $\%V_{bur}$ describes the volume occupied by any given ligand inside a sphere with a 3.5 Å radius around the metal center and topographical steric maps [4] are created using SambVca 2.1 package [5]. Since its introduction, the $\%V_{bur}$ parameter has proven to be useful as a descriptor of iTMCs in catalysis [6–9]. In the field of iTMC-based lighting devices, however, it has not gained attention despite its potential in structural analysis.

Heteroleptic copper(I)-based iTMCs have been employed in light-emitting electrochemical cells (LECs) and represent a promising avenue towards cost-efficient and sustainable lighting devices [10–12]. Consequently, understanding of the photophysical behavior of these complexes has guided their improved design for applications in LECs [13–18]. Electronic properties such as redox potentials,

absorption and emission spectra are among the descriptors used in the analysis of Cu(I) complexes. Quantifiable descriptors of steric factors, however, are mostly limited to discussions regarding angles and/or bond-lengths in X-ray single crystal structures. We have recently evaluated the effect that Cu...O distances in the {Cu(POP)} and {Cu(xantphos)} domains of [Cu(P[^]P)(N[^]N)][X] (POP = bis(2-(diphenylphosphanyl)phenyl)ether; xantphos = 4,5-bis(diphenylphosphanyl)-9,9-dimethyl-9H-xanthene) compounds have on solid-state photoluminescence quantum yield (PLQY) values [19]. Discussions regarding steric shielding of the copper(I) complex cation by the ligands are mostly limited to simplistic comparisons of steric bulk imposed by ligand-substituents [19–27]. Therefore, we sought to investigate the usefulness of %V_{bur} with regard to Cu(I)-based iTMCs in lighting devices. As a case study we chose [Cu(NN)(PP)]⁺ systems (where NN and PP refer to bidentate diimine and mono- or bi-dentate bisphosphane ligands) due to its popularity and photoluminescence quantum yields (PLQYs) because of the importance of large PLQY values for lighting purposes.

2. Results and discussion

2.1. General strategies

The Cambridge Structural Database (CSD) [28] was searched for compounds consisting of mononuclear [Cu(NN)(PP)]⁺ units where NN and PP refer to diimine and bisphosphane ligands. Searches were made using CSD version 5.4.1 and ConQuest version 2.0.4. [29]. The results were then further reduced to compounds with reported solid-state photoluminescence quantum yields (PLQYs). Particularly, values for thin-film PLQYs were not included as such values can differ from PLQYs of powder or crystal samples [11,18,25]. Moreover, PLQY values for crystalline samples were chosen over powder samples where such differentiations were made [30]. Similarly, PLQY values obtained under air were chosen over values obtained under an Ar atmosphere where such differentiations were made [31]. A total of 100 compounds were found and their %V_{bur} was calculated for the (NN), (PP) and (NN)(PP) units which are referred to as %V_{bur}(NN), %V_{bur}(PP) and %V_{bur}(NN + PP) (Table S1, supporting information) [17–21,23–27,30–48]. All compounds contain bidentate diimine and bisphosphane ligands with one exception containing a bidentate diimine and two monodentate triphenylphosphano ligands (CCDC: 1558486) [45]. Where a compound contained more than one independent cation in the asymmetric unit, the %V_{bur} values were calculated for each independent cation, resulting in a total of 123 data points for 100 compounds. An inherent bias is present in these values as compounds with low PLQYs may be inevitably not fully investigated or reported with regards to solid state PLQY values and X-ray single crystal structures. Furthermore, the spread of %V_{bur} is biased by virtue of the commercial availability of ligands, the synthetic feasibility of ligand scaffolds as well as the synthetic feasibility of different [Cu(NN)(PP)]⁺ complexes. As the PLQY values were measured by different groups or by different means, those values may thus be subject to varying errors. Consequently, we assume an error of ±10% of a given PLQY value, e.g., ±5% for a PLQY of 50%. The end result of an analysis for a given compound is summarized in Figure 1 for the archetypical [Cu(bpy)(xantphos)]⁺ (**1**) (bpy = 2,2'-bipyridine). Topographical steric maps for the (NN), (PP) and (NN)(PP) subunits are shown including the total %V_{bur} as well as the %V_{bur} for the four quadrants. The topographical steric maps plot the metal at the center of the reference axes (X, Y) splitting the plot into four quadrants. The volume occupied by the ligands is indicated by contour lines (Z axis) where positive values refer to the upper hemisphere of the sphere.

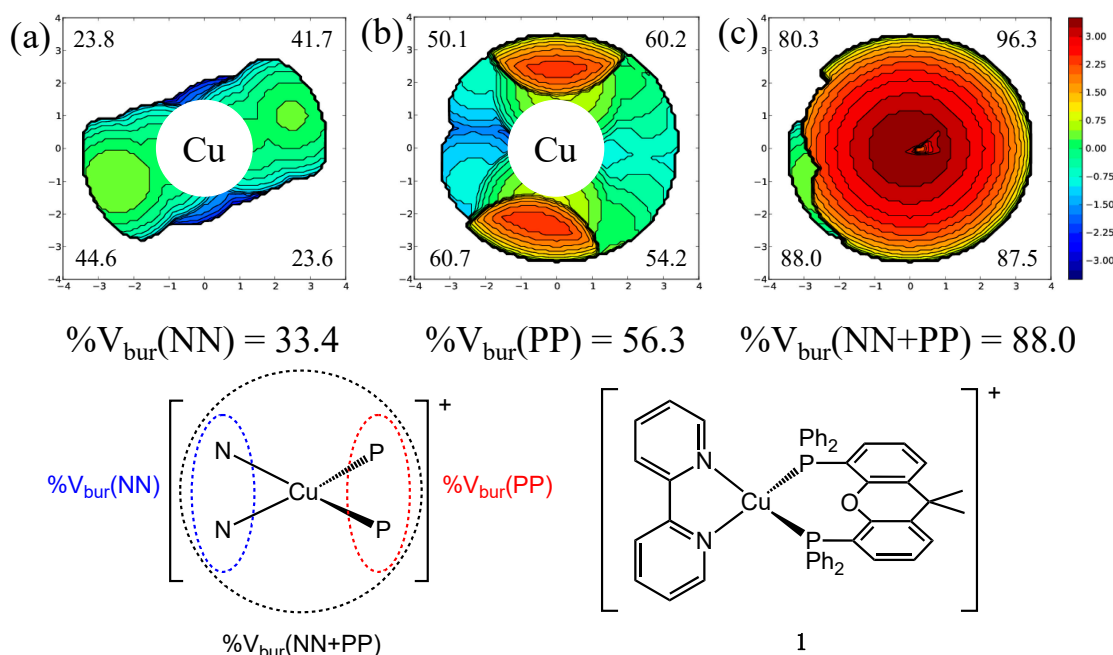


Figure 1. Topographical steric maps for bpy (a), xantphos (b) and for {(bpy)(xantphos)} (c) of [Cu(bpy)(xantphos)]⁺ (1) and a schematic representation of (NN), (PP) and (NN)(PP) subunits indicated in dotted lines used for the calculations of the respective percent volume buried (%V_{bur}). Values in the corners of the topographical steric maps refer to the %V_{bur} of the respective quadrants and the total %V_{bur} are listed below. Axes of the topographical steric maps (in Å) refer to the X and Y reference axes and the Z axis is indicated by the contour lines (positive values refer to the upper hemisphere).

2.2. Macroscopic level

Scatter plots of the results for all 123 data points of the 100 compounds are shown in Figure 2. Careful analysis of these scatter plots suggests that, firstly, there is a small positive impact of increased %V_{bur}(NN) on the PLQY (Figure 2a), and, second, an optimal %V_{bur}(PP) seems to be located at ca 56%. An increase or decrease of %V_{bur}(PP) negatively impacts the PLQY (Figure 2b). Thirdly, similar to %V_{bur}(PP), there seems to be an optimal %V_{bur}(NN + PP) located at ca 92% (Figure 2c). The fourth point is that %V_{bur}(NN + PP) strongly depends on %V_{bur}(PP) while the %V_{bur}(NN) has little impact (Figure 2d–f).

For a more detailed analysis of the results, color-coded three-dimensional scatter plots were generated including all four variables (Figure 3 and Figure S1–S3, Supplementary Materials). The PLQY was plotted against two %V_{bur} values with the remaining third %V_{bur} color-coded in the scatter plots. All three iterations of such plots support the dependence of large %V_{bur}(NN + PP) for large PLQYs as seen in Figure 2c. Furthermore, these plots reveal that the best outcome is achieved by a shared %V_{bur} between the NN and PP ligands. A large %V_{bur}(NN + PP) relying mostly on the PP ligand, on the other hand, yields low PLQYs. This shared contribution from both ligand units to the %V_{bur}(NN + PP) seems to be the cause for the above mentioned observation regarding a perceived optimal %V_{bur}(PP) at ca 56%. Most likely, a shared contribution of %V_{bur}(NN) and %V_{bur}(PP) within the [Cu(NN)(PP)]⁺ framework is more difficult to achieve for %V_{bur}(PP) > 60% resulting in only three data-points in that regime. At this point it should be mentioned again that the values presented here are biased by synthetic feasibility and only serve to reflect empirical trends in reported values and the usefulness of %V_{bur}.

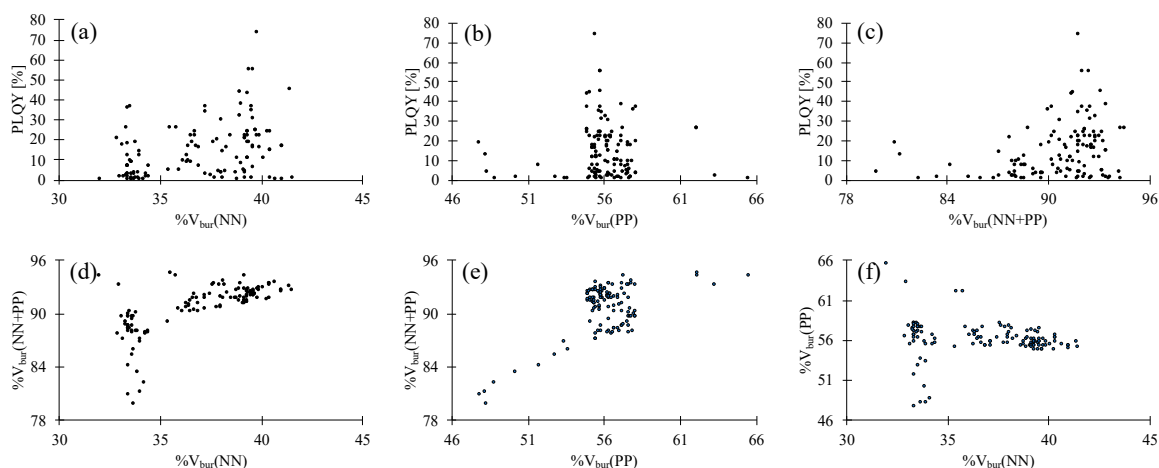


Figure 2. Scatter plots of photoluminescence quantum yield (PLQY), $\%V_{\text{bur}}(\text{NN})$, $\%V_{\text{bur}}(\text{PP})$ and $\%V_{\text{bur}}(\text{NN} + \text{PP})$ for all 100 compounds [17–21,23–27,30–48]. (a) Scatter plot of PLQY vs. $\%V_{\text{bur}}(\text{NN})$. (b) Scatter plot of PLQY vs. $\%V_{\text{bur}}(\text{PP})$. (c) Scatter plot of PLQY vs. $\%V_{\text{bur}}(\text{NN} + \text{PP})$. (d) Scatter plot of $\%V_{\text{bur}}(\text{NN})$ vs. $\%V_{\text{bur}}(\text{NN} + \text{PP})$. (e) Scatter plot of $\%V_{\text{bur}}(\text{PP})$ vs. $\%V_{\text{bur}}(\text{NN} + \text{PP})$. (f) Scatter plot of $\%V_{\text{bur}}(\text{NN})$ vs. $\%V_{\text{bur}}(\text{PP})$.

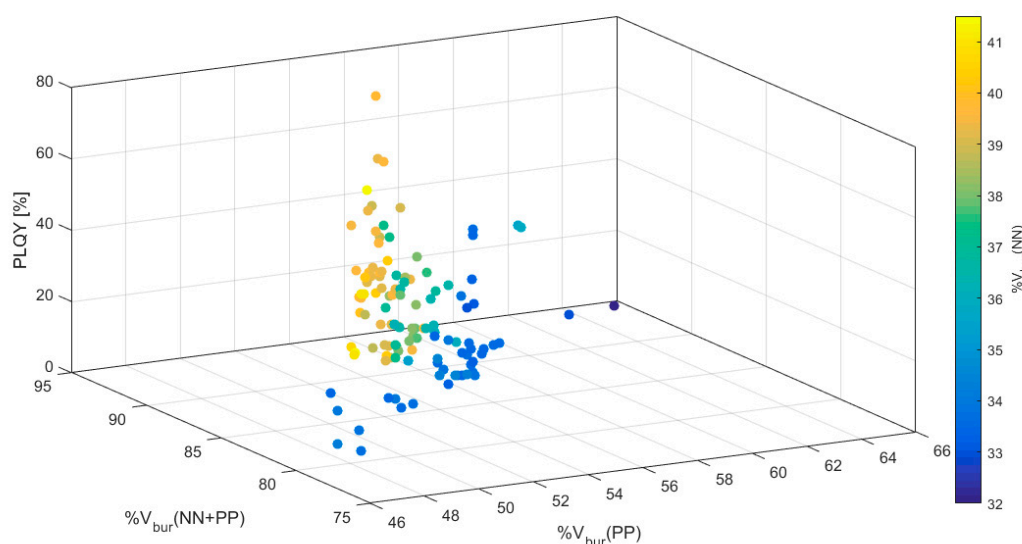


Figure 3. 3-Dimensional scatter plot with color-coded $\%V_{\text{bur}}(\text{NN})$ of all 100 compounds found in the Cambridge Structural Database (CSD) (Table S1, Supplementary Materials) [17–21,23–27,30–48].

2.3. Case Study 1: Importance of Steric Effects

In 2018, we reported twelve copper(I) complexes with 6-alkoxy- or 6-alkylthio-substituted bpy ligands in combination with xantphos (**2a–7a**) or POP (**2b–7b**) (Figure 4) [26]. The complexes were investigated by means of single crystal X-ray analysis, NMR spectroscopy, absorption and emission spectra, cyclic voltammetry as well as excited state lifetime measurements and density functional theory (DFT) calculations. The observed PLQY values (Table 1) were analyzed and a trend was established of increased PLQY by increased rigidity of xantphos compared to POP as well as increased steric bulk of the NN ligand in the order of $\text{bpyXMe} < \text{bpyXEt} < \text{bpyXPh}$ ($\text{X} = \text{O}, \text{S}$). However, $\%V_{\text{bur}}$ is not included in this discussion and the explanation as such is only partially supported by the reported values (compare PLQYs of **2a** and **4a** or **2b** and **4b**). Thus, the available photophysical properties in combination with the relatively large set of substrates renders this set of compounds a suitable case study for the inclusion of $\%V_{\text{bur}}$ as a descriptor in the discussion of photophysical properties.

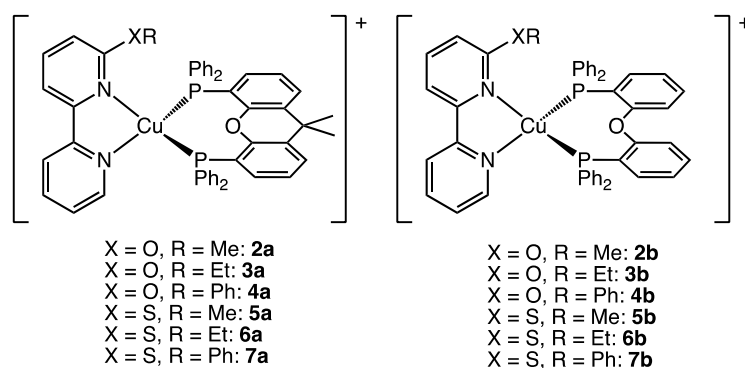


Figure 4. Structures of the $[\text{Cu}(\text{NN})(\text{PP})]^+$ cations reported in reference [26] and used in case study 1.

The PLQY values for the series of complexes shown in Figure 4 as well as $\%V_{\text{bur}}$ are summarized in Table 1 and Figure 5. An analysis of the $\%V_{\text{bur}}(\text{NN})$ values shows that the intuitive assignment of increased steric bulk in the order of $\text{bpyXMe} < \text{bpyXEt} < \text{bpyXPh}$ ($\times = \text{O}, \text{S}$) is not reflected in the percent volume buried. Instead the following order is more appropriate based on the calculated $\%V_{\text{bur}}(\text{NN})$:

For $\text{P}^{\wedge}\text{P} = \text{Xantphos}$: $\text{bpyOPh} < \text{bpyOMe} \approx \text{bpyOEt} < \text{bpySEt} \approx \text{bpySPh} \approx \text{bpySMe}$

For $\text{P}^{\wedge}\text{P} = \text{POP}$: $\text{bpyOPh} < \text{bpyOMe} \approx \text{bpyOEt} < \text{bpySPh} \approx \text{bpySMe} < \text{bpySEt}$

Overall, the $\%V_{\text{bur}}(\text{PP})$ values for POP are larger than those for xantphos with the exception of compounds **7a** and **7b**. Moreover, $\%V_{\text{bur}}(\text{NN} + \text{PP})$ seems to increase with $\%V_{\text{bur}}(\text{NN})$ while the largest $\%V_{\text{bur}}(\text{NN} + \text{PP})$ appears to be located at a medium $\%V_{\text{bur}}(\text{PP})$ of ca. 56.5%. Visualization of all four properties in color-coded three-dimensional scatter plots reveals that the highest PLQY values are reached when a high $\%V_{\text{bur}}(\text{NN} + \text{PP})$ is achieved by a combination of high $\%V_{\text{bur}}(\text{NN})$ and $\%V_{\text{bur}}(\text{PP})$ (Figure 6), in agreement with the interpretation of all 100 compounds (*vide supra*). Notably, comparing **5a** or **6a** to **7a** shows an increased PLQY with an increased $\%V_{\text{bur}}(\text{PP})$ or $\%V_{\text{bur}}(\text{NN} + \text{PP})$ while a similar correlation is not present when comparing **5a** to **6a** which only differ in $\%V_{\text{bur}}(\text{NN})$. Consequently, the nature of the differing PLQYs when comparing **5a** and **6a** is not due to the steric effects of the particular ligand system. Alternative explanations may be based on crystal packing such as improved accessibility of atmospheric O_2 to the complex [20].

Table 1. Reported PLQY values for powder samples for Cu(I) complexes and $\%V_{\text{bur}}$ for (NN), (PP), and (NN)(PP) units. Data are from reference [26].

Complex	PLQY [%]	$\%V_{\text{bur}}(\text{NN})$	$\%V_{\text{bur}}(\text{PP})$	$\%V_{\text{bur}}(\text{NN} + \text{PP})$
2a	19	36.6	56.3	91.8
2b	17	36.4	57.0	91.0
3a	22	36.7	56.4	92.2
3b	9	36.3	57.2	91.2
4a	12	36.3	55.5	90.7
4b ^a	5	35.4/35.9	55.1/57.7	89.1/90.6
5a	21	39.2	56.1	92.8
5b	30	38.0	56.3	90.7
6a	32	38.9	56.1	92.8
6b	22	38.5	56.5	91.8
7a	38	39.0	57.2	93.4
7b	20	37.8	55.7	90.7

^a Two crystallographically independent cations are present in the asymmetric unit.

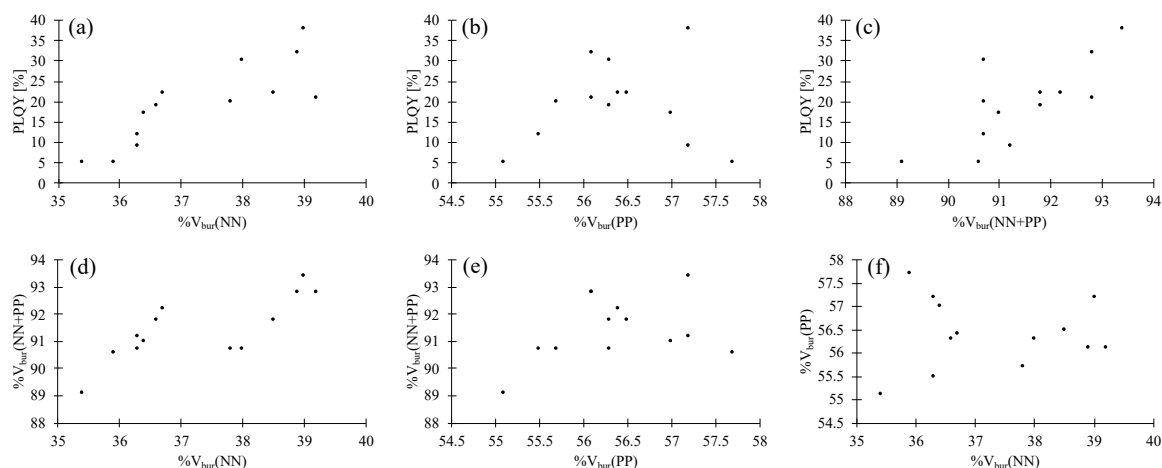


Figure 5. Scatter plots of PLQY, %V_{bur}(NN), %V_{bur}(PP) and %V_{bur}(NN + PP) for compounds **2a/b–7a/b** [26]. (a) Scatter plot of PLQY vs. %V_{bur}(NN). (b) Scatter plot of PLQY vs. %V_{bur}(PP). (c) Scatter plot of PLQY vs. %V_{bur}(NN + PP). (d) Scatter plot of %V_{bur}(NN) vs. %V_{bur}(NN + PP). (e) Scatter plot of %V_{bur}(PP) vs. %V_{bur}(NN + PP). (f) Scatter plot of %V_{bur}(NN) vs. %V_{bur}(PP).

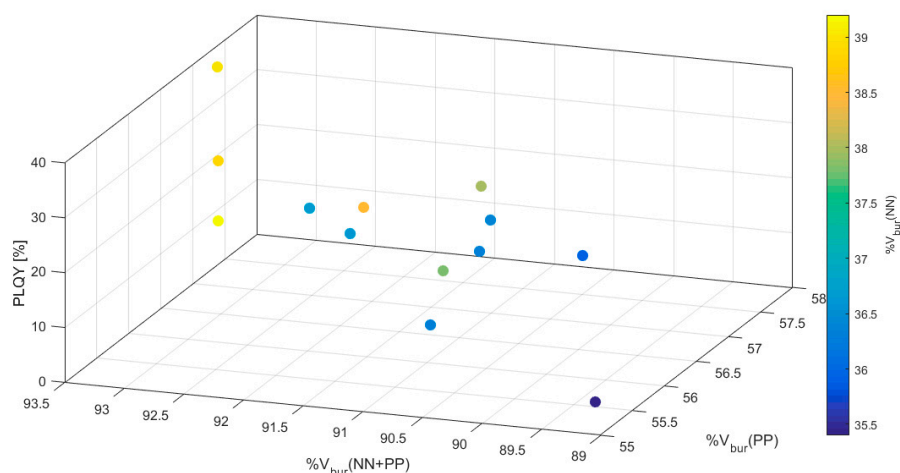


Figure 6. 3-Dimensional scatter plot with color-coded %V_{bur}(NN) for compounds **2a/b–7a/b** [26].

2.4. Case Study 2—Investigating Electronic Effects

Tsubomura and co-workers reported a series of seven heteroleptic copper(I) complexes in 2015 with the aim of investigating oxygen-responsive luminescence in the solid state. The single crystal X-ray structures of compounds **8–12** (Figure 7) were reported as well as powder PLQY values under air and under an argon atmosphere (Table 2) [31]. Given the choice of N[^]N and P[^]P ligands made by the authors, it is assumed that differences in PLQY are mostly due to electronic effects with the exception of **8** and **10**. The authors rationalize the trends in the observed PLQYs through differences in the crystal packing preventing structural rearrangement and differences in the transitions based on DFT calculations. Special emphasis was placed on the presence of voids in the crystal lattices which allows for excited state quenching by atmospheric O₂. While significant differences in shielding by the ligands of the central copper(I) cation are not expected, we considered that an analysis of %V_{bur} may provide further insight. Most importantly, %V_{bur} values allow for a straight-forward, quantitative comparison of steric effects if these are indeed present.

An analysis of the scatter plots in Figure 8 indicates that steric effects may participate in the decrease of PLQY in the case of **8** and **10**. The remaining compounds are almost identical in the %V_{bur} values and any differences in PLQY may be attributed to electronic effects. On the other hand, effects due to differences in crystal packing can be excluded as changes in PLQY under air or under Ar

atmosphere are absent or negligible. Only complex **10** exhibits a significant increase in PLQY upon removal of atmospheric O₂. Structural shielding by the ligand system for compound **10** may be present but is negated by the presence of voids in the crystal packing and effective quenching of the excited state by O₂ and energy transfer occurs instead. The lack of change in the PLQYs for the remaining compounds may be explained by structural rigidity inferred by the crystal packing rather than shielding of the central copper(I) cation.

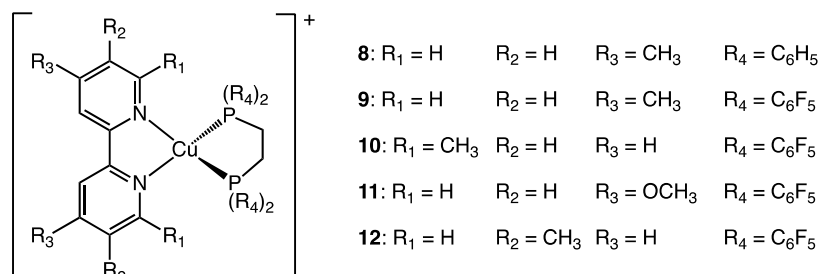


Figure 7. Structures of complexes **8–12** studied by Tsubomura and co-workers in 2015 [31].

Table 2. Reported PLQY values for powder samples for copper(I) complexes and %V_{bur} for (NN), (PP), and (NN)(PP) units. Data are from reference [31].

Complex	PLQY [%]	%V _{bur} (NN)	%V _{bur} (PP)	%V _{bur} (NN + PP)
8	0.5 (0.5) ^a	34.2	48.8	82.3
9	7 (8) ^a	34.4	55.6	88.0
10	0.5 (9) ^a	41.0	55.0	92.5
11	3 (3) ^a	34.3	55.5	87.7
12^b	2 (2) ^a	34.3/34.4	56.6/56.2	87.9/87.9

^aValue in parenthesis is for sample under Ar atmosphere. ^bTwo crystallographically independent cations are present in the asymmetric unit.

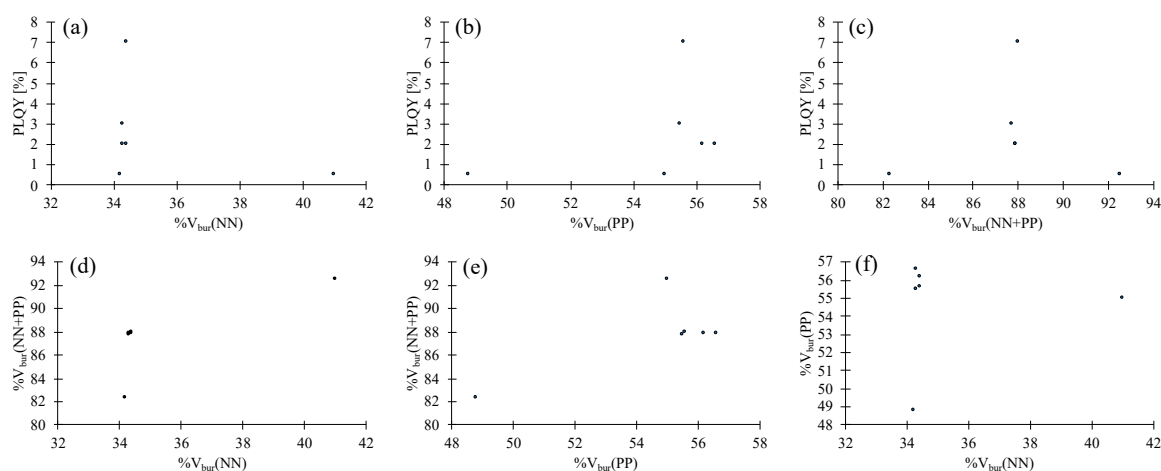


Figure 8. Scatter plots of PLQY, %V_{bur}(NN), %V_{bur}(PP) and %V_{bur}(NN + PP) for compounds **8–12** [31].

(a) Scatter plot of PLQY vs. %V_{bur}(NN). (b) Scatter plot of PLQY vs. %V_{bur}(PP). (c) Scatter plot of PLQY vs. %V_{bur}(NN + PP). (d) Scatter plot of %V_{bur}(NN) vs. %V_{bur}(NN + PP). (e) Scatter plot of %V_{bur}(PP) vs. %V_{bur}(NN + PP). (f) Scatter plot of %V_{bur}(NN) vs. %V_{bur}(PP).

2.5. Case Study 3—Differentiating Steric from Electronic Factors

In 2016, two of us reported a series of heteroleptic [Cu(NN)(PP)]⁺ complexes with 6- or 6,6'-substituted bpy ligands in combination with POP or xantphos (**13–18**, Figure 9) [18]. Following investigations of the structural and photophysical properties, the complexes were tested in LECs and were also investigated using DFT calculations. While high PLQY values were obtained for complexes

13, **14**, **16** and **17** (Figure 9), it was observed that replacing the Me or Et substituent with a Ph group resulted in a significantly lower PLQY (Table 3). We ascribed this sharp drop in PLQY to a lower T_1 state leading to increased feasibility of non-radiative decay pathways for **15** and **18**. We note that the structural discussions in the original publication did not provide a conclusive relationship between steric effects on the observed PLQYs. While % V_{bur} does not yield any insight into electronic effects, it does offer a concise overview of possible steric effects.

Analysis of the % V_{bur} values does not result in a clear correlation between the shielding of the central Cu(I) cation and PLQY values (Table 3). Graphical representation of these values further shows that the observed low PLQYs for **15** and **18** do not fit any possible correlation (Figure 10). Lastly, color-coded three-dimensional scatter plots clearly reveal that large PLQY values are obtained by virtually any combination of % V_{bur} with no correlation (Figure 11) as opposed to the correlations seen in case study 1 or in the analysis of all 100 complexes. This further supports the original hypothesis of lowered PLQY values due to a lowered T_1 state by virtue of the phenyl substituent.

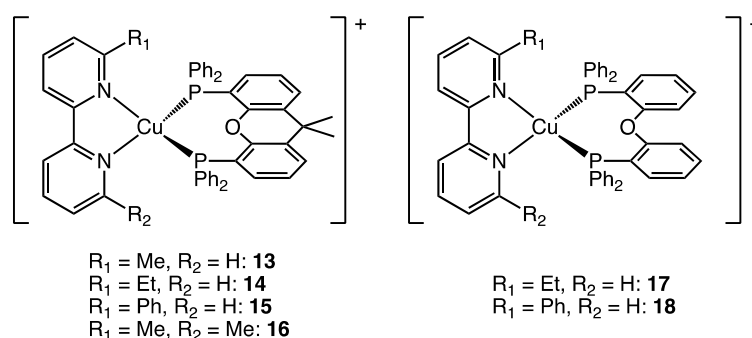


Figure 9. Structures of complexes **13**–**18** from reference [18].

Table 3. Reported PLQY values for powder samples for copper(I) complexes and % V_{bur} for (NN), (PP), and (NN)(PP) units. Data are from reference [18].

Complex	PLQY [%]	% $V_{bur}(\text{NN})$	% $V_{bur}(\text{PP})$	% $V_{bur}(\text{NN} + \text{PP})$
13	34	37.2	55.9	91.8
14	37	37.2	55.8	92.0
15	3.7	39.2	57.3	94.2
16	37	39.5	54.9	92.5
17	24	36.7	55.7	90.4
18	5.2	39.1	55.4	91.2

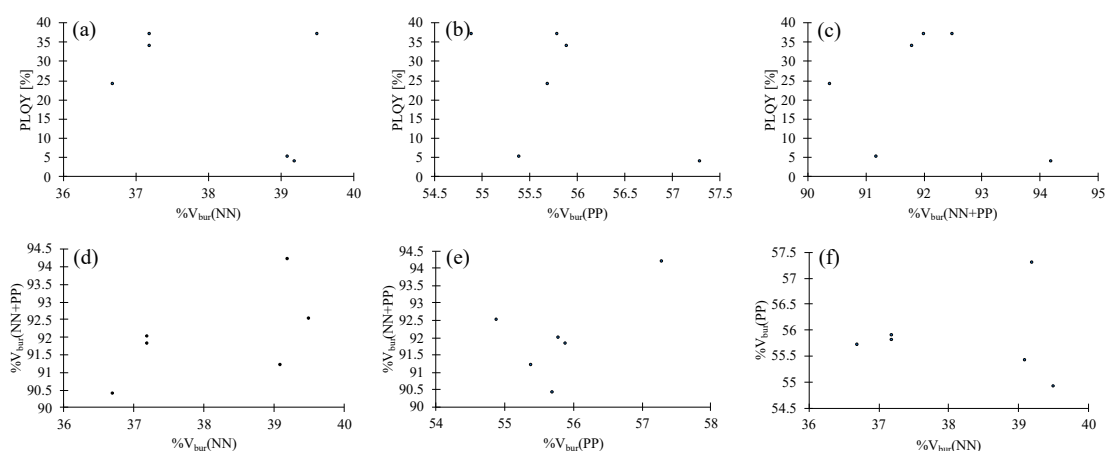


Figure 10. Scatter plots of PLQY, % $V_{bur}(\text{NN})$, % $V_{bur}(\text{PP})$ and % $V_{bur}(\text{NN} + \text{PP})$ for compounds **13**–**18** [18]. (a) Scatter plot of PLQY vs. % $V_{bur}(\text{NN})$. (b) Scatter plot of PLQY vs. % $V_{bur}(\text{PP})$. (c) Scatter plot of PLQY vs. % $V_{bur}(\text{NN} + \text{PP})$. (d) Scatter plot of % $V_{bur}(\text{NN})$ vs. % $V_{bur}(\text{NN} + \text{PP})$. (e) Scatter plot of % $V_{bur}(\text{PP})$ vs. % $V_{bur}(\text{NN} + \text{PP})$. (f) Scatter plot of % $V_{bur}(\text{NN})$ vs. % $V_{bur}(\text{PP})$.

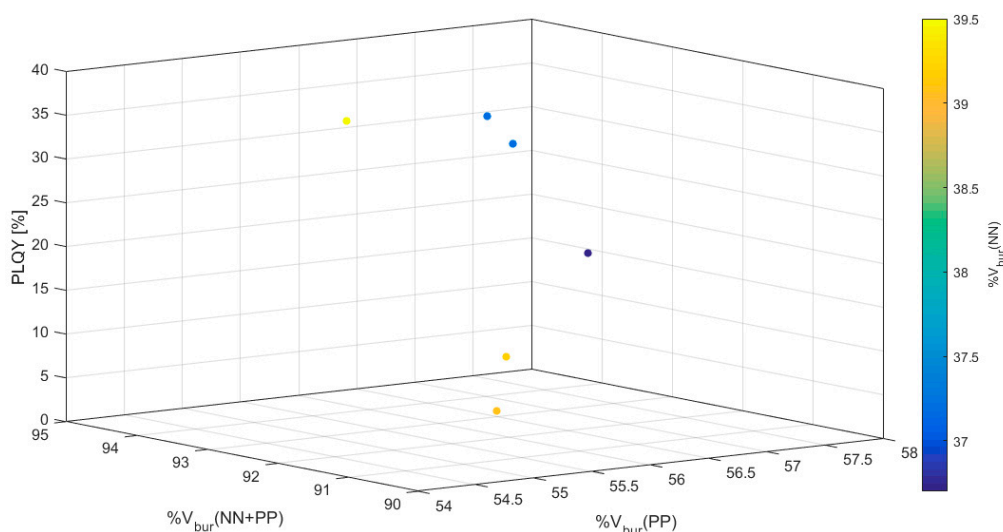


Figure 11. 3-Dimensional scatter plot with color-coded $\%V_{\text{bur}}(\text{NN})$ for compounds 13–18 [18].

3. Materials and Methods

The Cambridge Structural Database (CSD) [28] was searched for compounds consisting of mononuclear $[\text{Cu}(\text{NN})(\text{PP})]^+$. Searches were made using CSD version 5.4.1 and ConQuest version 2.0.4 [29]. Literature sources of the results were searched for reports of appropriate PLQY values which were collected together with the CIF files (Table S1 in the Supplementary Material). Topographical steric maps [4] were created using SambVca 2.1 package (<https://www.molnac.unisa.it/OMtools/sambvca2.1/index.html>) [5]. XYZ of the crystal structures were uploaded and the Cu(I) cation was defined as the center of the sphere. The negative Z-axis was defined by the N-atoms of the diimine for $\%V_{\text{bur}}(\text{NN})$ and $\%V_{\text{bur}}(\text{NN} + \text{PP})$ or by the P-atoms of the bisphosphane for $\%V_{\text{bur}}(\text{PP})$. The P-atoms of the bisphosphane defined the XZ-plane for $\%V_{\text{bur}}(\text{NN})$ and $\%V_{\text{bur}}(\text{NN} + \text{PP})$ and the N-atoms of the diimine for $\%V_{\text{bur}}(\text{PP})$. All atoms, except for the diimine ligand, bisphosphane ligand or both ligands, were deleted to calculate $\%V_{\text{bur}}(\text{NN})$, $\%V_{\text{bur}}(\text{PP})$ and $\%V_{\text{bur}}(\text{NN} + \text{PP})$, respectively. The Bondi radii were scaled by 1.17 and the sphere radius chosen as $r = 3.5 \text{ \AA}$. Mesh spacing of 0.10 \AA was used for the numerical integration and H-atoms were excluded.

4. Conclusions

We have demonstrated that values of $\%V_{\text{bur}}$ represent a means of quantifying relationships between structure and PLQYs of heteroleptic $[\text{Cu}(\text{NN})(\text{PP})]^+$ complexes. Using the CSD as a source of structural data, we were able to analyze 100 $[\text{Cu}(\text{NN})(\text{PP})]^+$ complexes for which solid state PLQYs and single-crystal X-ray structures were available; this provided 123 data points. Analysis of all complexes showed that PLQY values are the highest when $\%V_{\text{bur}}(\text{NN} + \text{PP})$ is maximized by an increased $\%V_{\text{bur}}(\text{NN})$ and $\%V_{\text{bur}}(\text{PP})$. Three case studies underline the potential usefulness of including $\%V_{\text{bur}}$ as an addition in the structural discussion of $[\text{Cu}(\text{NN})(\text{PP})]^+$ complexes as it relates to solid-state photophysical behavior.

Supplementary Materials: The following are available online: Figure S1–S3: 3-Dimensional scatter plot with color-coded $\%V_{\text{bur}}(\text{PP})$, $\%V_{\text{bur}}(\text{NN} + \text{PP})$ or PLQY of all 100 compounds found, Table S1: Reported PLQY values for powder samples for Cu(I) complexes and $\%V_{\text{bur}}$ for (NN), (PP), and (NN)(PP) units..

Author Contributions: Conceptualization, investigation, formal analysis, M.A.-Z.; manuscript draft: M.A.-Z., Manuscript editing and discussion of concepts and interpretation of data: C.E.H. and E.C.C. All authors have read and agreed to the published version of the manuscript.

Funding: There was no external funding for this project.

Acknowledgments: C.E.H. and E.C.C. thank the University of Basel for continued support. M.A.-Z. thanks Xile Hu for discussion.

Conflicts of Interest: The authors declare no conflict of interest.

References

1. Strohmeier, W.; Müller, F.-J. Klassifizierung phosphorhaltiger Liganden in Metallcarbonyl-Derivaten nach der π -Acceptorstärke. *Chemische Berichte* **1967**, *100*, 2812–2821, doi:10.1002/cber.19671000907.
2. Tolman, C.A. Steric effects of phosphorus ligands in organometallic chemistry and homogeneous catalysis. *Chem. Rev.* **1977**, *77*, 313–348, doi:10.1021/cr60307a002.
3. Poater, A.; Ragone, F.; Giudice, S.; Costabile, C.; Dorta, R.; Nolan, S.P.; Cavallo, L. Thermodynamics of N-Heterocyclic Carbene Dimerization: The Balance of Sterics and Electronics. *Organometallics* **2008**, *27*, 2679–2681, doi:10.1021/om8001119.
4. Poater, A.; Ragone, F.; Mariz, R.; Dorta, R.; Cavallo, L. Comparing the Enantioselective Power of Steric and Electrostatic Effects in Transition-Metal-Catalyzed Asymmetric Synthesis. *Chem. Eur. J.* **2010**, *16*, 14348–14353, doi:10.1002/chem.201001938.
5. Falivene, L.; Cao, Z.; Petta, A.; Serra, L.; Poater, A.; Oliva, R.; Scarano, V.; Cavallo, L. Towards the online computer-aided design of catalytic pockets. *Nature Chem.* **2019**, *11*, 872–879, doi:10.1038/s41557-019-0319-5.
6. Clavier, H.; Correa, A.; Cavallo, L.; Escudero-Adán, E.C.; Benet-Buchholz, J.; Slawin, A.M.Z.; Nolan, S.P. [Pd(NHC)(allyl)Cl] Complexes: Synthesis and Determination of the NHC Percent Buried Volume ($\%V_{bur}$) Steric Parameter. *Eur. J. Inorg. Chem.* **2009**, *2009*, 1767–1773, doi:10.1002/ejic.200801235.
7. Clavier, H.; Nolan, S.P. Percent buried volume for phosphine and N-heterocyclic carbene ligands: Steric properties in organometallic chemistry. *Chem. Commun.* **2010**, *46*, 841–861, doi:10.1039/B922984A.
8. Gómez-Suárez, A.; Nelson, D.J.; Nolan, S.P. Quantifying and understanding the steric properties of N-heterocyclic carbenes. *Chem. Commun.* **2017**, *53*, 2650–2660, doi:10.1039/C7CC00255F.
9. Cervantes-Reyes, A.; Rominger, F.; Hashmi, A.S.K. Sterically Demanding Ag^I and Cu^I N-Heterocyclic Carbene Complexes: Synthesis, Structures, Steric Parameters, and Catalytic Activity. *Chem. Eur. J.* **2020**, *26*, 5530–5540, doi:10.1002/chem.202000600.
10. Armaroli, N.; Accorsi, G.; Holler, M.; Moudam, O.; Nierengarten, J.-F.; Zhou, Z.; Wegh, R.T.; Welter, R. Highly Luminescent Cu^I Complexes for Light-Emitting Electrochemical Cells. *Adv. Mater.* **2006**, *18*, 1313–1316, doi:10.1002/adma.200502365.
11. Costa, R.D.; Tordera, D.; Ortí, E.; Bolink, H.J.; Schönle, J.; Graber, S.; Housecroft, C.E.; Constable, E.C.; Zampese, J.A. Copper(I) complexes for sustainable light-emitting electrochemical cells. *J. Mater. Chem.* **2011**, *21*, 16108–16118, doi:10.1039/C1JM12607E.
12. Costa, R.D.; Ortí, E.; Bolink, H.J.; Monti, F.; Accorsi, G.; Armaroli, N. Luminescent Ionic Transition-Metal Complexes for Light-Emitting Electrochemical Cells. *Angew. Chem. Int. Ed.* **2012**, *51*, 8178–8211, doi:10.1002/anie.201201471.
13. Hofbeck, T.; Monkowius, U.; Yersin, H. Highly Efficient Luminescence of $\text{Cu}(\text{I})$ Compounds: Thermally Activated Delayed Fluorescence Combined with Short-Lived Phosphorescence. *J. Am. Chem. Soc.* **2015**, *137*, 399–404, doi:10.1021/ja5109672.
14. Elie, M.; Sguerra, F.; Di Meo, F.; Weber, M.D.; Marion, R.; Grimault, A.; Lohier, J.-F.; Stallivieri, A.; Brosseau, A.; Pansu, R.B.; et al. Designing NHC–Copper(I) Dipyriddyamine Complexes for Blue Light-Emitting Electrochemical Cells. *ACS Appl. Mater. Interfaces* **2016**, *8*, 14678–14691, doi:10.1021/acsami.6b04647.
15. Hamze, R.; Shi, S.; Kapper, S.C.; Muthiah Ravinson, D.S.; Estergreen, L.; Jung, M.-C.; Tadde, A.C.; Haiges, R.; Djurovich, P.I.; Peltier, J.L.; et al. “Quick-Silver” from a Systematic Study of Highly Luminescent, Two-Coordinate, d10 Coinage Metal Complexes. *J. Am. Chem. Soc.* **2019**, *141*, 8616–8626, doi:10.1021/jacs.9b03657.

16. Hamze, R.; Peltier, J.L.; Sylvinson, D.; Jung, M.; Cardenas, J.; Haiges, R.; Soleilhavoup, M.; Jazzar, R.; Djurovich, P.I.; Bertrand, G.; et al. Eliminating nonradiative decay in Cu(I) emitters: >99% quantum efficiency and microsecond lifetime. *Science* **2019**, *363*, 601–606, doi:10.1126/science.aav2865.
17. Keller, S.; Constable, E.C.; Housecroft, C.E.; Neuburger, M.; Prescimone, A.; Longo, G.; Pertegás, A.; Sessolo, M.; Bolink, H.J. [Cu(bpy)(P[^]P)]⁺ containing light-emitting electrochemical cells: Improving performance through simple substitution. *Dalton Trans.* **2014**, *43*, 16593–16596, doi:10.1039/C4DT02847C.
18. Keller, S.; Pertegás, A.; Longo, G.; Martínez, L.; Cerdá, J.; Junquera-Hernández, J.M.; Prescimone, A.; Constable, E.C.; Housecroft, C.E.; Ortí, E.; et al. Shine bright or live long: Substituent effects in [Cu(N[^]N)(P[^]P)]⁺-based light-emitting electrochemical cells where N[^]N is a 6-substituted 2,2'-bipyridine. *J. Mater. Chem. C* **2016**, *4*, 3857–3871, doi:10.1039/C5TC03725E.
19. Keller, S.; Alkan-Zambada, M.; Prescimone, A.; Constable, E.C.; Housecroft, C.E. Extended π -Systems in Diimine Ligands in [Cu(P[^]P)(N[^]N)][PF₆] Complexes: From 2,2'-Bipyridine to 2-(Pyridin-2-yl)Quinoline. *Crystals* **2020**, *10*, 255, doi:10.3390/cryst10040255.
20. Smith, C.S.; Branham, C.W.; Marquardt, B.J.; Mann, K.R. Oxygen Gas Sensing by Luminescence Quenching in Crystals of Cu(xantphos)(phen)⁺ Complexes. *J. Am. Chem. Soc.* **2010**, *132*, 14079–14085, doi:10.1021/ja103112m.
21. Li, X.-L.; Ai, Y.-B.; Yang, B.; Chen, J.; Tan, M.; Xin, X.-L.; Shi, Y.-H. Syntheses, structures and photophysical properties of a series of luminescent copper(I) mixed-ligand complexes. *Polyhedron* **2012**, *35*, 47–54, doi:10.1016/j.poly.2011.12.040.
22. Tsubomura, T.; Kimura, K.; Nishikawa, M.; Tsukuda, T. Structures and photophysical properties of copper(I) complexes bearing diphenylphenanthroline and bis(diphenylphosphino)alkane: The effect of phenyl groups on the phenanthroline ligand. *Dalton Trans.* **2015**, *44*, 7554–7562, doi:10.1039/C5DT00835B.
23. Cabrera, A.R.; Gonzalez, I.A.; Cortés-Arriagada, D.; Natali, M.; Berke, H.; Daniliuc, C.G.; Camarada, M.B.; Toro-Labbé, A.; Rojas, R.S.; Salas, C.O. Synthesis of new phosphorescent imidoyl-indazol and phosphine mixed ligand Cu(I) complexes – structural characterization and photophysical properties. *RSC Adv.* **2016**, *6*, 5141–5153, doi:10.1039/C5RA20450J.
24. Brunner, F.; Martínez-Sarti, L.; Keller, S.; Pertegás, A.; Prescimone, A.; Constable, E.C.; Bolink, H.J.; Housecroft, C.E. Peripheral halo-functionalization in [Cu(N[^]N)(P[^]P)]⁺ emitters: Influence on the performances of light-emitting electrochemical cells. *Dalton Trans.* **2016**, *45*, 15180–15192, doi:10.1039/C6DT02665F.
25. Keller, S.; Brunner, F.; Junquera-Hernández, J.M.; Pertegás, A.; La-Placa, M.-G.; Prescimone, A.; Constable, E.C.; Bolink, H.J.; Ortí, E.; Housecroft, C.E. CF₃ Substitution of [Cu(P[^]P)(bpy)][PF₆] Complexes: Effects on Photophysical Properties and Light-Emitting Electrochemical Cell Performance. *ChemPlusChem* **2018**, *83*, 217–229, doi:10.1002/cplu.201700501.
26. Alkan-Zambada, M.; Keller, S.; Martínez-Sarti, L.; Prescimone, A.; Junquera-Hernández, J.M.; Constable, E.C.; Bolink, H.J.; Sessolo, M.; Ortí, E.; Housecroft, C.E. [Cu(P[^]P)(N[^]N)][PF₆] compounds with bis(phosphane) and 6-alkoxy, 6-alkylthio, 6-phenyloxy and 6-phenylthio-substituted 2,2'-bipyridine ligands for light-emitting electrochemical cells. *J. Mater. Chem. C* **2018**, *6*, 8460–8471, doi:10.1039/C8TC02882F.
27. Fresta, E.; Volpi, G.; Milanese, M.; Garino, C.; Barolo, C.; Costa, R.D. Novel Ligand and Device Designs for Stable Light-Emitting Electrochemical Cells Based on Heteroleptic Copper(I) Complexes. *Inorg. Chem.* **2018**, *57*, 10469–10479, doi:10.1021/acs.inorgchem.8b01914.
28. Groom, C.R.; Bruno, I.J.; Lightfoot, M.P.; Ward, S.C. The Cambridge Structural Database. *Acta Crystallogr.* **2016**, *B72*, 171–179.
29. Bruno, I.J.; Cole, J.C.; Edgington, P.R.; Kessler, M.; Macrae, C.F.; McCabe, P.; Pearson, J.; Taylor, R. New software for searching the Cambridge Structural Database and visualizing crystal structures. *Acta Crystallogr.* **2002**, *B58*, 389–397.
30. Linfoot, C.L.; Leitz, M.J.; Richardson, P.; Rausch, A.F.; Chepelin, O.; White, F.J.; Yersin, H.; Robertson, N. Thermally Activated Delayed Fluorescence (TADF) and Enhancing Photoluminescence Quantum Yields of [Cu^I(diimine)(diphosphine)]⁺ Complexes—Photophysical, Structural, and Computational Studies. *Inorg. Chem.* **2014**, *53*, 10854–10861, doi:10.1021/ic500889s.

31. Nishikawa, M.; Wakita, Y.; Nishi, T.; Miura, T.; Tsubomura, T. Long-lived and oxygen-responsive photoluminescence in the solid state of copper(i) complexes bearing fluorinated diphosphine and bipyridine ligands. *Dalton Trans.* **2015**, *44*, 9170–9181, doi:10.1039/C5DT00199D.
32. Keller, S.; Prescimone, A.; Bolink, H.; Sessolo, M.; Longo, G.; Martínez-Sarti, L.; Junquera-Hernández, J.M.; Constable, E.C.; Ortí, E.; Housecroft, C.E. Luminescent copper(i) complexes with bisphosphane and halogen-substituted 2,2'-bipyridine ligands. *Dalton Trans.* **2018**, *47*, 14263–14276, doi:10.1039/C8DT01338A.
33. Brunner, F.; Babaei, A.; Pertegás, A.; Junquera-Hernández, J.M.; Prescimone, A.; Constable, E.C.; Bolink, H.J.; Sessolo, M.; Ortí, E.; Housecroft, C.E. Phosphane tuning in heteroleptic $[\text{Cu}(\text{N}^{\wedge}\text{N})(\text{P}^{\wedge}\text{P})]^+$ complexes for light-emitting electrochemical cells. *Dalton Trans.* **2019**, *48*, 446–460, doi:10.1039/C8DT03827A.
34. Keller, S.; Prescimone, A.; Constable, E.C.; Housecroft, C.E. Copper(i) and silver(i) complexes of 9,9-dimethyl-4,5-bis(di-tert-butylphosphino)xanthene: Photophysical properties and structural rigidity under pressure. *Photochem. Photobiol. Sci.* **2018**, *17*, 375–385, doi:10.1039/C7PP00432J.
35. Brunner, F.; Graber, S.; Baumgartner, Y.; Häussinger, D.; Prescimone, A.; Constable, E.C.; Housecroft, C.E. The effects of introducing sterically demanding aryl substituents in $[\text{Cu}(\text{N}^{\wedge}\text{N})(\text{P}^{\wedge}\text{P})]^+$ complexes. *Dalton Trans.* **2017**, *46*, 6379–6391, doi:10.1039/C7DT00782E.
36. Mazzeo, F.; Brunner, F.; Prescimone, A.; Constable, E.C.; Housecroft, E.C. Intra-Cation versus Inter-Cation π -Contacts in $[\text{Cu}(\text{P}^{\wedge}\text{P})(\text{N}^{\wedge}\text{N})][\text{PF}_6]$ Complexes. *Crystals* **2020**, *10*, 1, doi:10.3390/cryst10010001.
37. Nohara, I.; Keller, A.; Tarassenko, N.; Prescimone, A.; Constable, E.C.; Housecroft, E.C. Heteroleptic $[\text{Cu}(\text{P}^{\wedge}\text{P})(\text{N}^{\wedge}\text{N})][\text{PF}_6]$ Compounds with Isomeric Dibromo-1,10-Phenanthroline Ligands. *Inorganics* **2020**, *8*, 4, doi:10.3390/inorganics8010004.
38. Keller, S.; Bantle, M.; Prescimone, A.; Constable, E.C.; Housecroft, E.C. Hinged and Wide: A New $\text{P}^{\wedge}\text{P}$ Ligand for Emissive $[\text{Cu}(\text{P}^{\wedge}\text{P})(\text{N}^{\wedge}\text{N})][\text{PF}_6]$ Complexes. *Molecules* **2019**, *24*, 3934, doi:10.3390/molecules24213934.
39. Murray, N.S.; Keller, S.; Constable, E.C.; Housecroft, C.E.; Neuburger, M.; Prescimone, A. $[\text{Cu}(\text{N}^{\wedge}\text{N})(\text{P}^{\wedge}\text{P})]^+$ complexes with 2,2':6',2''-terpyridine ligands as the $\text{N}^{\wedge}\text{N}$ domain. *Dalton Trans.* **2015**, *44*, 7626–7633, doi:10.1039/C5DT00517E.
40. Weber, M.D.; Viciano-Chumillas, M.; Armentano, D.; Cano, J.; Costa, R.D. σ -Hammett parameter: A strategy to enhance both photo- and electro-luminescence features of heteroleptic copper(I) complexes. *Dalton Trans.* **2017**, *46*, 6312–6323, doi:10.1039/C7DT00810D.
41. Nishikawa, M.; Tsubomura, T. Photophysical Properties of a Copper(I) Complex Bearing 4,4'-Dimethoxy-2,2'-bipyridine and 1,3-Bis(diphenylphosphino)propane. *Bull. Chem. Soc. Jpn.* **2014**, *87*, 912–914, doi:10.1246/bcsj.20140069.
42. Arnosti, N.; Brunner, F.; Susic, I.; Keller, S.; Junquera-Hernández, J.M.; Prescimone, A.; Bolink, H.J.; Sessolo, M.; Ortí, E.; Housecroft, C.E.; et al. Remote Modification of Bidentate Phosphane Ligands Controlling the Photonic Properties in Their Complexes: Enhanced Performance of $[\text{Cu}(\text{RN-xantphos})(\text{N}^{\wedge}\text{N})][\text{PF}_6]$ in Light-Emitting Electrochemical Cells. *Adv. Optical Mater.* **2020**, 1901689, doi:10.1002/adom.201901689.
43. González, I.A.; Henríquez, M.A.; Cortés-Arriagada, D.; Natali, M.; Daniliuc, C.G.; Dreyse, P.; Maze, J.; Rojas, R.S.; Salas, C.O.; Cabrera, A.R. Heteroleptic Cu(i) complexes bearing methoxycarbonyl-imidoylindazole and POP ligands – an experimental and theoretical study of their photophysical properties. *New J. Chem.* **2018**, *42*, 12576–12586, doi:10.1039/C8NJ00699G.
44. Yang, M.; Li, X.-N.; Jia, J.-H.; Chen, X.-L.; Lu, C.-Z. A rationally designed vapoluminescent compound with adsorptive channels and responsive luminophores for volatile organic compounds (VOCs). *Dalton Trans.* **2019**, *48*, 1179–1183, doi:10.1039/C8DT04360D.
45. Zhu, N.; Wang, G.; Lin, S.; Li, Z.-F.; Xin, X.-L.; Yang, Y.-P.; Liu, M.; Jin, Q.-H. New discovery in crystallography: Correlation of terahertz time-domain spectra with crystal structures and photoluminescence properties of mononuclear/binuclear diimine–Cu(i)-phosphine complexes. *CrystEngComm* **2019**, *21*, 4275–4288, doi:10.1039/C9CE00729F.
46. Kuang, X.-N.; Lin, S.; Liu, J.-M.; Han, H.-L.; Liu, M.; Xin, X.-L.; Yang, Y.-P.; Li, Z.-F.; Jin, Q.-H.; Li, S.-F.; et al. Heteroleptic Cu(I) complexes with aromatic diimines and phosphines: Synthesis, structure, photophysical properties and THz time domain spectroscopy. *Polyhedron* **2019**, *165*, 51–62, doi:10.1016/j.poly.2019.03.003.

47. Liu, R.; Huang, M.-M.; Yao, X.-X.; Li, H.-H.; Yang, F.-L.; Li, X.-L. Synthesis, structures and aggregation-induced emissive properties of copper(I) complexes with 1H-imidazo[4,5-f][1,10]phenanthroline derivative and diphosphine as ligands. *Inorg. Chim. Acta* **2015**, *434*, 172–180, doi:10.1016/j.ica.2015.05.019.
48. Meyer, M.; Brunner, F.; Prescimone, A.; Constable, E.C.; Housecroft, C.E. Chimera Diimine Ligands in Emissive [Cu(P[^]P)(N[^]N)][PF₆] Complexes. *Inorganics* **2020**, *8*, 33, doi:10.3390/inorganics8050033.

Sample Availability: No new compounds were prepared in this work; no samples are available from the authors.



© 2020 by the authors. Licensee MDPI, Basel, Switzerland. This article is an open access article distributed under the terms and conditions of the Creative Commons Attribution (CC BY) license (<http://creativecommons.org/licenses/by/4.0/>).